Near-Infrared Fluorescence Lifetime pH-Sensitive Probes

Mikhail Y. Berezin,[†] Kevin Guo,[†] Walter Akers,[†] Ralph E. Northdurft,[†] Joseph P. Culver,[†] Bao Teng,[§] Olga Vasalatiy,[§] Kyle Barbacow,[§] Amir Gandjbakhche,[¶] Gary L. Griffiths,[§] and Samuel Achilefu[†‡*]

[†]Department of Radiology and [‡]Department of Biochemistry and Molecular Biophysics, Washington University School of Medicine, St. Louis, Missouri; and [§]Imaging Probe Development Center, National Heart, Lung, and Blood Institute and [¶]Physical Biology Program, Eunice Shriver National Institute of Child Health and Human Development, National Institutes of Health, Bethesda, Washington, District of Columbia

ABSTRACT We report what we believe to be the first near-infrared pH-sensitive fluorescence lifetime molecular probe suitable for biological applications in physiological range. Specifically, we modified a known fluorophore skeleton, hexamethylindotricarbocyanine, with a tertiary amine functionality that was electronically coupled to the fluorophore, to generate a pH-sensitive probe. The pK_a of the probe depended critically on the location of the amine. Peripheral substitution at the 5-position of the indole ring resulted in a compound with $pK_a \sim 4.9$ as determined by emission spectroscopy. In contrast, substitution at the meso-position shifted the pK_a to 5.5. The resulting compound, LS482, demonstrated steady-state and fluorescence-lifetime pH-sensitivity. This sensitivity stemmed from distinct lifetimes for protonated (~1.16 ns in acidic DMSO) and deprotonated (~1.4 ns in basic DMSO) components. The suitability of the fluorescent dyes for biological applications was demonstrated with a fluorescence-lifetime tomography system. The ability to interrogate cellular processes and subsequently translate the findings in living organisms further augments the potential of these lifetime-based pH probes.

INTRODUCTION

pH-sensitive fluorescent probes are widely used to report the acidic status of a variety of cellular compartments (1). This approach has been applied to in vivo imaging of diseases associated with elevated acidity level (2,3). High acidity levels (acidemia and acidosis) have been implicated in a number of systemic pathologies (4), such as renal acidosis, metabolic disorders, intoxications, diabetes, and emphysema, as well as localized hyperacidity such as infections, inflammation, and cancer. In particular, solid tumors with pH ranging from 5.8 to 7.7 (5,6) on average are 0.5 units lower than the pH of normal tissue due to a high level of anaerobic metabolism. The tight control of intracellular pH requires removal of the excess acidic products from tumor cells to the extracellular-extravascular space due to the poor lymphatic drainage in cancer tissue (7). This significant difference in pH between normal and surrounding provides a unique opportunity to image the metabolic status of cancerous tissue using optical imaging with a suitable pH indicator. To be used in vivo, the indicator should preferably be optically active within a relatively narrow near-infrared (NIR) region (700–900 nm) and possess a pK_a within physiologically relevant range, which we loosely defined between 4.8 and 7.8 (8). Interest in molecular probes with these features has recently spurred the synthesis of novel NIR pH indicators that have had success in vitro, with potential for in vivo imaging applications (9–16).

There are several different mechanisms by which a fluorescent probe can indicate a change in environmental pH. The prevalent approach utilizes substantial enhancement or quenching of fluorescence intensity or a shift of excitation and/or emission wavelength peak that responds maximally at the pH close to a probes' pK_a value. However, fluorescence intensity measurements are difficult to quantify in heterogeneous tissue and recorded intensity changes may be due to a concentration gradient instead of differences in tissue pH values. Spectral shifts are more reliable and quantitative in microscopy but developing NIR fluorescent probes with pH-induced distinct spectral shift between 700 and 900 nm represents a synthetic challenge. Moreover, fluorescence intensity measurements for such molecular systems are also subject to wavelength-dependent heterogeneities in biological tissues.

In contrast to intensity, the fluorescence lifetime of a probe is largely independent from concentration and has been introduced as in vivo optical imaging modality to overcome the problem of concentration dependence and also enhance contrast and alleviate some other typical problems associated with intensities including scattering (17), sample turbidity, and autofluorescence (18–20). Recently, several articles describing lifetime pH-sensitive probes such as quantum dots (21), fluorescent proteins (22), and the mechanism of their sensing have been published. Despite the advantages of fluorescence lifetime and the long lifetime appreciated by microscopists in cell imaging, several limitations hinder the broad acceptance of the method for in vivo imaging. In the past, the lack of correlation between fluorescence lifetime of the probes and the tissue environment, engineering challenges inherent to deep tissue imaging, and long acquisition and data processing time have hampered the recognition of fluorescent lifetime imaging as an in vivo method. Recently, significant

Submitted December 28, 2010, and accepted for publication February 23, 2011.

*Correspondence: achilefus@mir.wustl.edu

Editor: David E. Wolf.

0006-3495/11/04/2063/10 $2.00

doi: 10.1016/j.bpj.2011.02.050

advances in the design of fluorescent-environment-sensitive lifetime probes (23–25), high-speed electro-optic instrumentation (26), and fast postacquisition time (27) have turned fluorescence lifetime in vivo imaging into a practical tool.

Herein, we report the design and synthesis of NIR fluorescence lifetime pH-sensitive fluorophores and lifetime pH imaging using diffuse optical fluorescence lifetime tomography. We demonstrate that two NIR fluorophores, LS479 and LS482 (Fig. 1), have marked pH-sensitivity through steady-state and fluorescence lifetime measurements. The pH sensitivity of LS479, initially synthesized as a fluorogenic metal chelator (28), was found by serendipity while studying the pH stability of metal complexes. Although LS479 was pH-sensitive, its low pK_a value led to the synthesis of LS482, which has a higher pK_a value in the physiologically important range. Moreover, LS482 exhibited a large variance in lifetime between acidic and basic forms, providing a foundation for pH lifetime imaging. Using fluorescence lifetime diffuse optical tomography (26), we demonstrate that phantoms composed of LS482 at three different pH values, implanted in a mouse, have lifetimes similar to those obtained from in vitro measurements. Thus, the combination of a pH-sensitive fluorescence lifetime molecular probe and a fluorescence lifetime diffuse optical tomography (FL-DOT) system allowed us to establish the foundation for the practical application of fluorescence lifetime pH imaging in the NIR region.

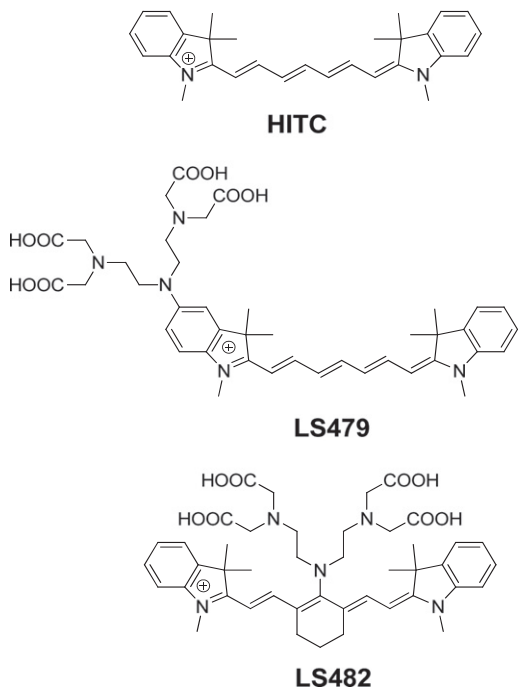

FIGURE 1 Structures of NIR dyes used in this study. LS479 is an HITC analog with DTPA conjugated to the indole group while LS482 has DTPA conjugated to the meso position.

MATERIALS AND METHODS

Steady-state optical measurements

Absorption spectra were recorded on a DU 640 UV-visible spectrophotometer (Beckman-Coulter, Brea, CA) and fluorescence spectra were recorded on a Fluorolog-3 spectrofluorometer (Horiba Jobin Yvon, Edison, NJ). For LS479 and LS482, excitation was at 675 nm, with emission scan from 690 to 950 nm. All fluorescence measurements were conducted at room temperature. For titrations, the compounds were predissolved in dimethylsulfoxide (DMSO) and added to water (30 mL) so the total concentration of the dye did not exceed 0.2 absorbance units. Titration was conducted with stirring under Ar atmosphere to exclude CO_2 interference. The solution was initially basified with dilute aqueous NaOH and the desired pH was attained by titrating the solution with diluted aqueous HCl. The acidification of the solution was conducted at relatively constant ionic strengths ($I = 0.1$ M provided by 0.1 M NaCl in water). The pH of the solution was continuously measured using an Accumet pH meter AB15 (Fisher Scientific, Pittsburgh, PA) equipped with a liquid-filled, Ag/AgCl reference pH/ATC double-junction combination Accumet electrode.

At each pH point, absorption and fluorescent measurements were determined. The pK_a values were calculated from the sigmoidal dose-response curve fit implemented in software Prism 5.0 (GraphPad Software, La Jolla, CA). Contour plots of fluorescence intensity versus excitation wavelength versus emission wavelength of the dye solutions at different pH were generated with excitation scanning from 560 to 780 nm with 2 nm intervals. The simultaneous changes in emission from 680 to 880 nm with 1 nm intervals at pH = 3.0 and 8.0 were recorded and the data were plotted using SigmaPlot 11.0 software (Systat Software, Chicago, IL). Quantum yields at different representative pH were measured relative to indocyanine green in DMSO ($\Phi = 0.12$) at 700 nm excitation (29).

Titrations using fluorescence lifetime measurement

Fluorescence lifetimes (FLT) were measured using time-correlated single-photon-counting (Horiba) with a 700-nm excitation source NanoLed (impulse repetition rate 1 MHz) at 90° to the detector (Hamamatsu Photonics, Hamamatsu City, Japan). For the FLT measurements, the dyes were dissolved in water and the absorbance of the measured solutions was maintained below 0.15 at a 700-nm excitation wavelength. The detector was set to 780 nm with a 26-nm bandpass and data collected until the peak signal reached 10,000 counts. The FLT was recorded on a 50-ns scale. The instrument response function was obtained using a Rayleigh scatter of Ludox-40 (0.05% in Milli-Q water; Sigma-Aldrich, St. Louis, MO) in an acrylic transparent cuvette at 700-nm emission. Decay analysis software (DAS6 v6.1; Horiba) was used for lifetime calculations. The goodness of fit was judged by χ^2 values, Durbin-Watson parameters, as well as visual observations of fitted line, residuals, and autocorrelation functions. For titrations, the dyes were dissolved in DMSO and acidified with dilute trifluoroacetic acid (TFA) or basified with dilute triethylamine (TEA). The resulting DMSO solutions were diluted with 0.1 M NaCl aqueous solution (1:1 vol), the pH of the solution was measured (pH_m) and corrected for dilution using the following equation:

$$pH = pH_m - \log_{10}2.$$

Synthesis of pH-sensitive probes

Synthesis of LS479 was described in a previous publication (28).

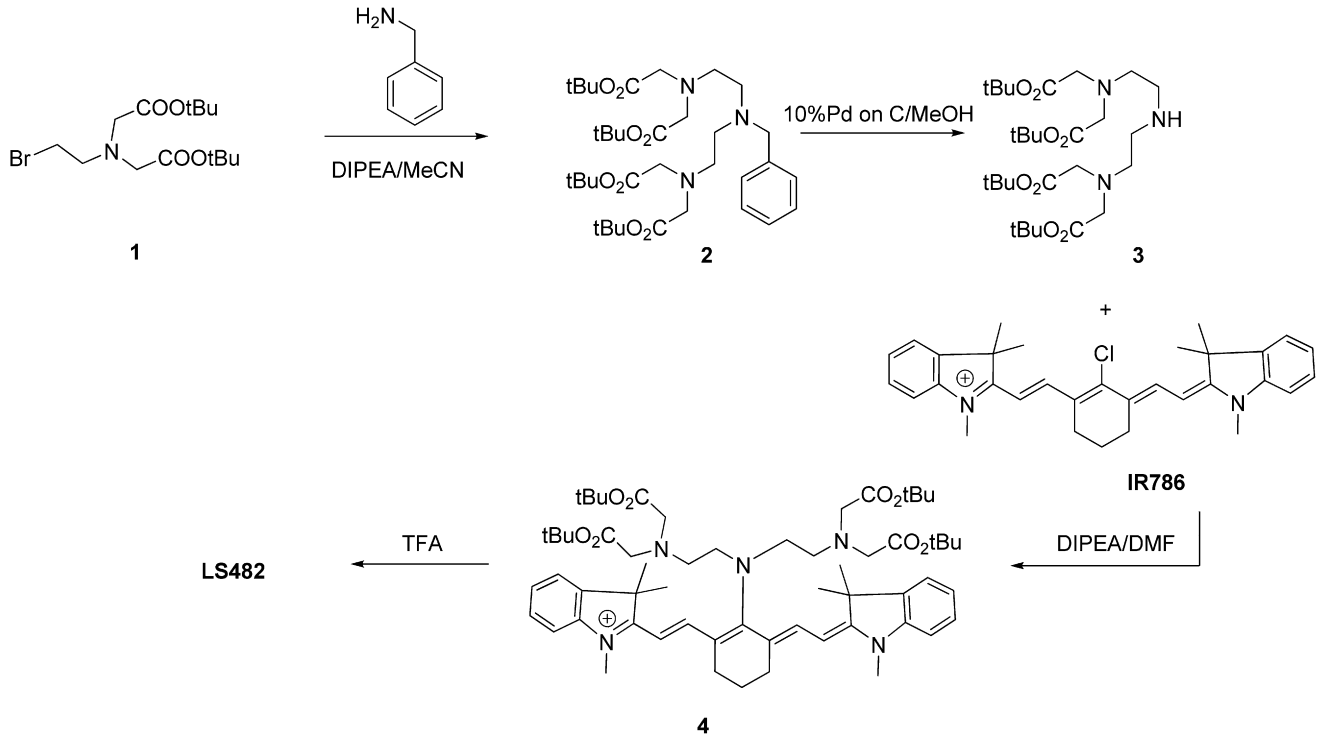

SCHEME 1

For the preparation of LS482, benzylamine was N-alkylated with the bromo derivative 1 (see Scheme 1) using *n*,*n*-diisopropylethylamine as a base in acetonitrile to obtain Compound 2. Intermediate 3 was prepared by removal of the benzyl protective group by hydrogenolysis with hydrogen and 10% palladium on carbon in methanol. N-alkylation of N,N″-tetrakis(t-butyloxycarbonylmethyl)-diethylenetriamine 3 with IR 786 perchlorate using *n*,*n*-diisopropylethylamine as a base in anhydrous dimethylformamide provided Compound 4. The yield of the reaction is somewhat moderate (10%), which might be attributed to steric hindrance around the secondary amine, as compared to the higher reaction yields seen with a primary amine (76%) (30). Isolation of Compound 4 from the reaction mixture was performed by preparative high-performance liquid chromatography. Removal of *t*-butyl protective groups under standard conditions using TFA gave target LS482. Details of the synthesis are given in the Supporting Material.

Fluorescence-lifetime tomography system

Animal studies were conducted on a recently developed temporally resolved fluorescence tomography system (26). Briefly, a pulsed Ti:S laser source with spectral filtering (80 MHz, 785 nm, <100-fs pulse width, 60 mW) was used for illumination. The beam, after passing through the focusing lens, was steered by a pair of galvanometer scanning mirrors to the source side of an imaging cassette. Light emitted from the detector plane of the imaging cassette was collected by a lens and temporally gated by an ultrafast gated image intensifier and detected by an electron-multiplying charge-coupled device camera for read-out. Optional filters in front of the lens allow acquisition of either the transmitted excitation or fluorescence emission (832 ± 10 nm). Timing between the source and the gated detection was controlled by a programmable delay unit allowing a series of images to capture the light emission as a function of time. A scan resulted in a temporal profile of transmitted excitation and stimulated emission at each detector location. From these data, we reconstructed a map of fluorescence yield and lifetime simultaneously via a normalized Born approach (31,32). Specifically, we used an analytical solution to the diffusion equation that incorporated absorption and scattering in the light model (33).

Lifetime tomography imaging

Male nude mice 6–12 weeks in age were used for in vivo imaging. Before scanning, each mouse was anesthetized with a mixture of ketamine (87 mg/kg) and xylazine (13 mg/kg) via intraperitoneal and subcutaneous injection for initial and sustained sedation, respectively. The mouse was then suspended vertically within the fluid-filled imaging cassette for the duration of the scan, as previously described. LS482 in acidic (DMSO-TFA), neutral (neat DMSO), and basic (DMSO-TEA) solutions were loaded into thin-walled sealed straws 3-mm in diameter and 10-mm long. Dye concentration was selected so that all three tubes had comparable fluorescence emission at 830 nm. The tubes were implanted ~1 mm below the skin surface in the subcutaneous space via a 5-mm incision on the dorsal aspect of each flank. Skin incisions were closed with tissue adhesive (Nexabond; Abbott Animal Health, Chicago, IL). Twenty-four time gates over a 20 × 3 source grid with 2-mm separation were imaged, covering a total area of 4.0 cm × 0.6 cm. The acquisition time for the entire set of data was ~5 min for excitation and 74 min for emission.

RESULTS

In vitro studies

pH-dependent optical probe LS479

Our initial efforts to develop an NIR lifetime probe focused on pH-sensitive properties of the previously described LS479 (28), a fluorescent dye with a covalently linked metal chelating group (Fig. 1). The probe showed low toxicity in mice, even at a relatively large dose of 15 mg/kg body

weight. Previous studies showed that the molecular probes do not have observable side effects in rodents during the two-month study period (34). LS479 is structurally similar to a known dye 1,1′,3,3,3′,3′-hexamethylindotricarbocyanine (HITC), which is widely used in analytical chemistry and biological optical imaging studies (35,36). The chelating group of LS479 was derived from diethylenetriaminepentaacetic acid (DTPA). A characteristic feature of LS479 compared to HITC is the presence of an amine functionality electronically coupled with the fluorophore. The electron pair on the amine is known to affect fluorescence and a number of pH-sensitive compounds, including NIR dyes, have utilized amino groups as fluorescence intensity pH-sensitive sensors (11,37–39).

Indeed, the steady-state titration absorbance and fluorescence spectra (Fig. 2, *A* and *B*) showed that LS479 was pH-sensitive. A similar analysis of HITC is described below and in the Supporting Material. An isosbestic point at 575 nm in the absorption spectra (Fig. 2 *A*) suggests the presence of protonated and deprotonated forms (40). Under basic (pH $>$ 7) conditions, the absorption band exhibited a moderate increase in peak intensity of ~25% from pH 3 to pH 8. In contrast, the fluorescence intensity increased substantially (Fig. 2 *B*), indicating that the deprotonated form of LS479 was more fluorescent than the protonated form (see Table 1 for quantum yields). A plot of intensity as a function of excitation and emission wavelength (constructed by scanning excitation wavelengths) demonstrated the presence of only one fluorescent form (Fig. 3). Acid dissociation constants (pK_a), computed from titration diagrams, were generated from acid-base absorption and steady-state emission experiments (Fig. 2 *C*). The pK_a in the ground state was found to be 4.45 $\pm$ 0.097 while the pKa in the excited state was found to be 4.93 $\pm$ 0.099, suggesting moderate photobasicity (41,42). Although the pK_a of the ground state is lower than the pH of most cells, the excited state pK_a is at the fringe of lysosomal pH of 4.8. However, these pH values narrows down the potential, in vivo, application of LS479 to extremely low pH organelles of cells.

The pH dependence of the probes was investigated in dilute solutions ($<$100 μM). At higher concentrations, a number of nonlinear optical effects, such as quenching due to aggregation, inner filter effect, and reabsorption can occur, causing a significant change in the emission lifetimes (43). In a biological system, however, the aggregation is minimal due to a variety of opsonization factors and the relatively low concentration of molecules injected into animals.

To expand the application to other cellular compartments and less acidic tissue environments, we explored the effect of pH on the fluorescence lifetime of LS479. We measured the lifetime in DMSO rather than in aqueous solutions. The use of DMSO as a solvent simulates in vivo environment more realistically than water because DMSO polarity is closer to that of blood and tissues (44). Hence, the lifetime of LS479 was measured in neat, acidified, and basified

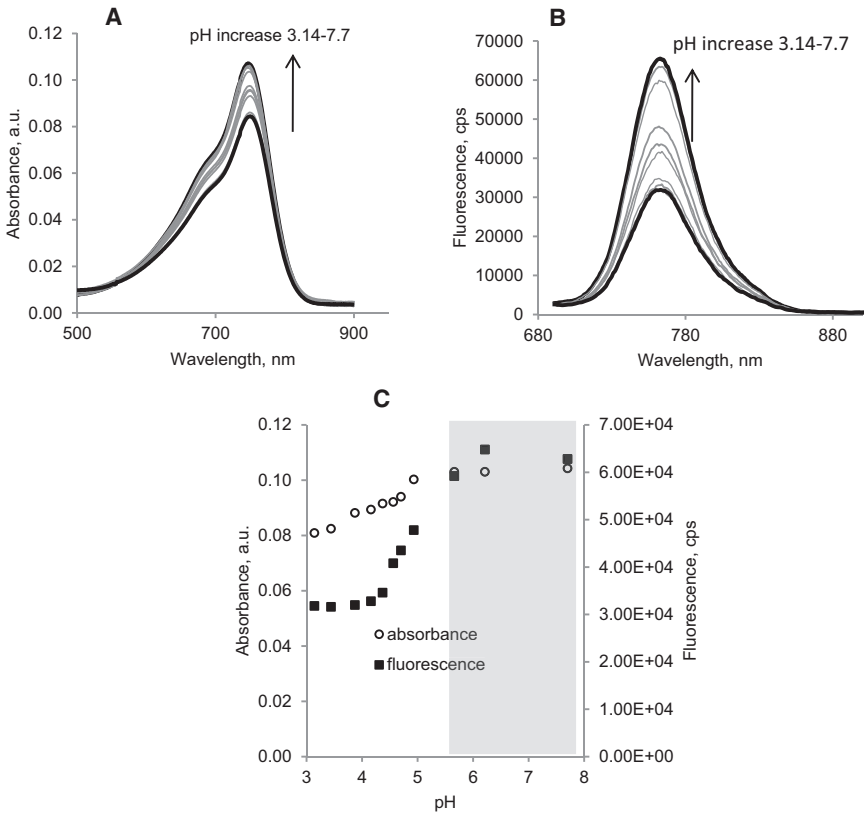

FIGURE 2 Absorption (*A*) and emission (*B*) titration spectra of LS479 in 0.1 M NaCl aqueous solutions, excitation/emission: 675:690–950 nm. (*C*) Titration diagrams of LS479 were generated from fluorescence and absorbance spectra. Acid dissociation constants were computed with the software Prism (GraphPad Software): pK_a in the ground state from the absorbance data is 4.45 $\pm$ 0.097 and pK_a* in the excited state from the emission data is 4.93 $\pm$ 0.099. *R* values were $>$0.99. Desired physiological range is shown in gray.

TABLE 1 Photophysical characteristics of studied dyes in aqueous solutions (excitation/emission: 700:715–950 nm)

Entry	pH*	λ_{abs} max, nm	$\varepsilon \times 10^{-3}$, M^{-1} cm^{-1}†	λ_{em} max, nm	ψ‡
LS479	3	750	83	762	0.008
	8	747	105	762	0.042
LS482	3	760	105	760	0.037
	8	710	84	793	0.101
HITC	3	736	250	771	0.113
	8	736	250	771	0.106

*Buffers, pH 3 and pH 8 (Hydrion; Micro Essential Laboratory, Brooklyn, NY).
†Molar absorptivities at the absorption maximum.
‡Quantum yield measured relative to indocyanine green in DMSO ($\psi = 0.12$).

DMSO. Fluorescence decays in neat and basified DMSO solutions were largely monoexponential (>96% of one component from two-exponential fit) and exhibited similar calculated fluorescence lifetimes of 0.77–0.78 ns (Table 2). Unfortunately, we were not able to determine the fluorescence lifetime at lower pH accurately because of a very weak fluorescence signal below the pK_a level.

LS482 as a pH-dependent optical probe with biologically suitable pK_a

To improve the low pK_a of LS479 and overcome potential problems associated with low fluorescence signal of protonated species, we synthesized LS482, where DTPA was placed in the meso position. This compound was subjected to the same set of steady-state and lifetime titration experiments as LS479 and the results are given in Figs. 3 and 4 as well as Tables 1 and 2. We found that LS482 displayed pH-sensitivity in all three categories: absorption, fluorescence intensity, and—most importantly—fluorescence lifetime. The changes upon protonation-deprotonation were reversible (Fig. S1 in the Supporting Material), indicating chemical stability of both forms.

Similar to LS479, the absorbance and fluorescence of LS482 decreased under acidic conditions and amplified (×10) at higher pH. Compared to LS479, the meso-substituted LS482 exhibited more intense fluorescence. The brightness of LS482, measured as a product of molar absorptivity and quantum yield ($\varepsilon \times \psi$), was 2.5–4.6 times higher than LS479 at corresponding pH values based on data from Table 1. Higher brightness is beneficial in optical imaging in vivo because it allows for lower dosage of a probe and the use of lower laser output. Analysis of the titration spectra (for the ground and excited states diagram; see Fig. 4 *C*) revealed that the acid dissociation constant of LS482 was shifted toward a more physiologically relevant range with ground (pK_a) and the excited (pK_a*) states pK_a of ~5.5.

In contrast to LS479, LS482 exhibited absorption (50 nm) and fluorescence (33 nm) bathochromic shifts upon acidification, suggesting the presence of two distinct fluorescence species, as illustrated by emission versus excitation contour plots (Fig. 3). The shift in spectra indicated a prominent alteration in chromophore structure upon protonation. Fluorescence lifetime measurements at different pH levels in

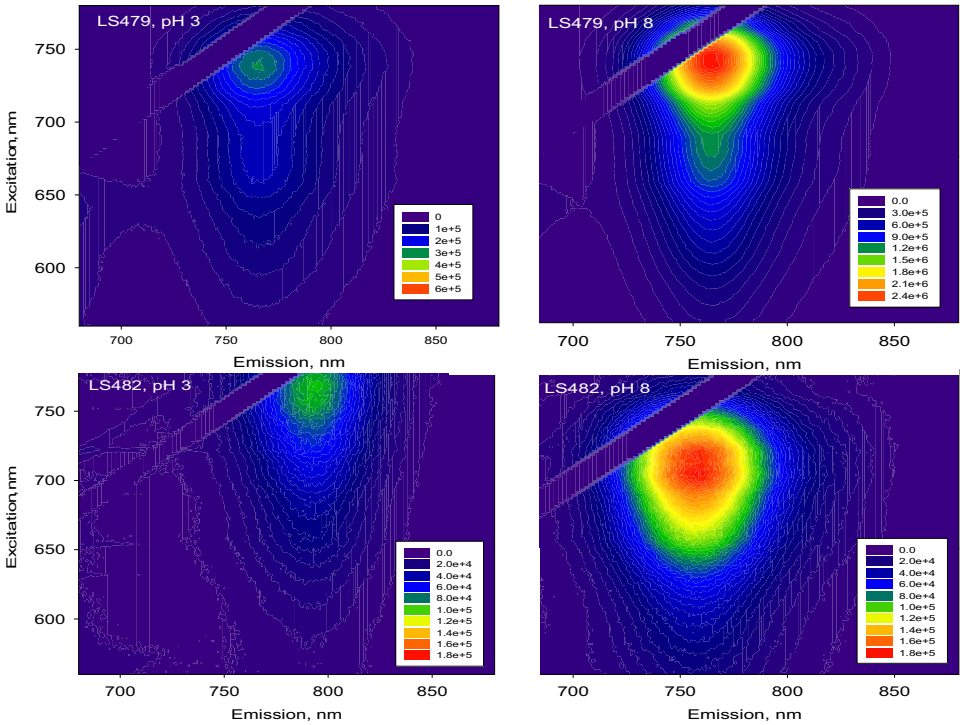

FIGURE 3 Contour plots representations emission versus excitation of LS479 and LS482 in two different aqueous media, acidic (pH = 3) and basic (pH = 8). The intensity of the fluorescence signals are shown in pseudo colors in the online version. Note that the scale for LS479 at pH 3 is four-times higher for better visualization. Excitation was scanned within 560–780 nm range with 2 nm steps; emission was collected from 680 to 880 nm with 1-nm intervals. Rayleigh signals were digitally removed (a stripe 20-nm-wide corresponding to Rayleigh scattering is seen in *upper-left corner* of each plot).

TABLE 2 Fluorescence lifetime of LS482 and HITC in DMSO solvent of differing acidity (excitation/emission: 700:780 nm, two-exponential fit)

Entry	pH	Species	τ_{AH}, ns	f_{AH}, %	τ_A, ns	f_A, %	$\tilde{\tau}$, ns	χ^2
	3.70*	*AH*			n/d†			
LS479	4.95	*AH*+*A*	0.78	96.8	—	—	0.78	1.35
	8.33	*A*	0.77	97.0	—	—	0.77	1.29
	3.94	*AH*	1.18	98. 1	—	—	1.18	1.25
LS482	5.52	*AH*+*A*	1.25‡	98.1	—	—	1.25	1.33
	8.60	*A*	—	—	1.39	98.3	1.39	1.31
	2.50	*A*	—	—	1.43	101.5	1.43	1.06
HITC	5.30	*A*	—	—	1.42	100.0	1.42	1.08
	11.5	*A*	—	—	1.42	101.2	1.42	1.08

*The pH of DMSO solution was determined after diluting it with 0.1 M NaCl(aq) (1:1 vol).

†Fluorescence intensity in acidic DMSO was too low for lifetime measurement.

‡The values correspond to a mixture of protonated *AH* and deprotonated *A* forms.

DMSO solution confirmed the two components with significantly different lifetimes of ~1.16 ns for protonated (*AH*, pH $<$ 4) and ~1.40 ns (*A*, pH $>$ 8) for nonprotonated species. As expected, the structurally similar HITC, which lacks an amine-coupled chromophore system, did not show any lifetime pH sensitivity (Table 2).

The fluorescence of both protonated and deprotonated forms of LS482 allowed us to construct a fluorescence lifetime titration curve (Fig. 4 *D*) and estimate the $pK_a^*{}_\tau$ solely based on the fluorescence lifetime. The determined $pK_a^*{}_\tau = 5.39$ was similar to the pK_a values determined by steady-state methods.

Fluorescence lifetime tomography

Having established that LS482 possesses lifetime pH-sensitive properties, we tested the feasibility of measuring pH-dependent lifetime using previously reported time-resolved diffuse optical tomography, which can simultaneously measure fluorescence intensity (yield) and lifetime (26). Due to the differential phase method, the system was able to measure short fluorescence lifetimes typical for NIR cyanine probes 0.35–2 ns with high precision (± 5 ps).

To demonstrate the feasibility of measuring fluorescence lifetimes at different pH levels in animals, we adopted a known approach of implanting phantoms into mice (14,26). Following this approach, we encapsulated solutions of LS482 in aqueous DMSO at pH 2.3, 5.7, and 8.1. The capsules were placed in the hindquarters of mice. The results of the imaging conducted in intensity and lifetime modes are shown in Fig. 5, *A* and *B*, correspondingly. The intensity map revealed that three phantoms had no functional information regarding the local milieu. In contrast, fluorescence lifetime imaging clearly indicated the presence

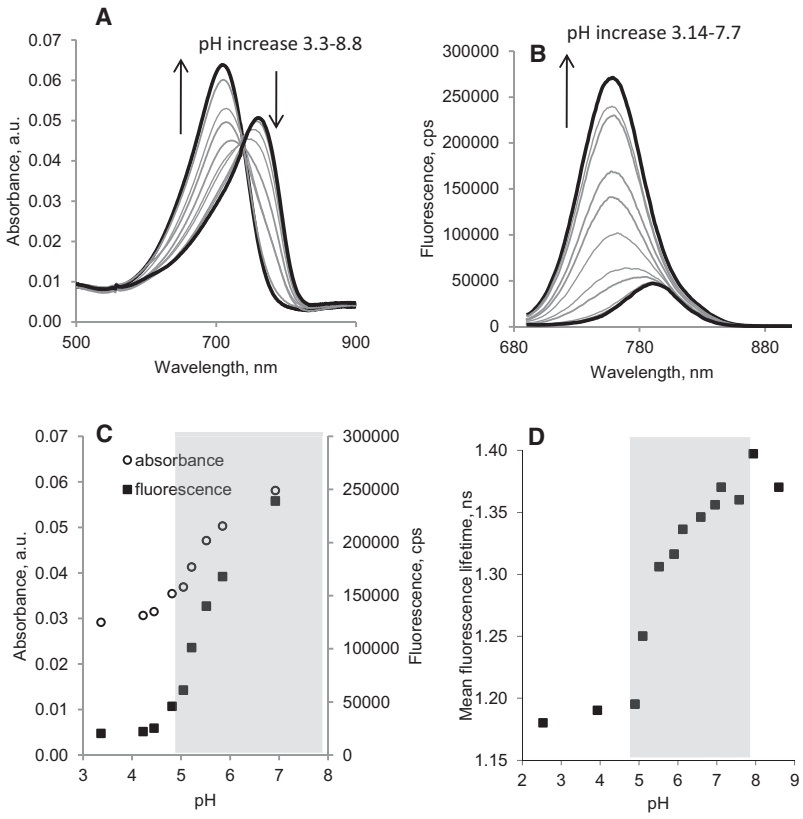

FIGURE 4 Absorption (*A*) and emission (*B*) spectra of LS482 in 0.1 M NaCl aqueous solutions at varying pH, excitation/emission: 675:690–900 nm. Steady-state titration diagram (*C*) was generated from absorption and emission spectra. Fluorescence lifetime titration diagram (*D*) was generated from measuring fluorescence lifetime of LS482 in acidic, neat, and basic DMSO. (Calculated pK_a: from absorption $pK_a = 5.47 \pm 0.053$, $R^2 = 0.99$, from emission $pK_a^* = 5.46 \pm 0.059$, $R^2 = 0.99$, from lifetime $pK_a{}^*{}_\tau = 5.39 \pm 0.09$, $R^2 = 0.98$.) Prism 5.0 (GraphPad Software) was used to determine the pK_a. Physiological range is shown in gray.

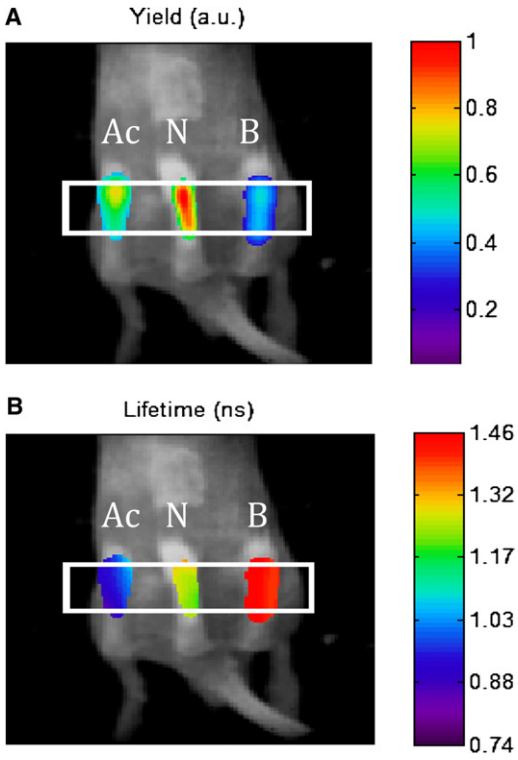

FIGURE 5 Fluorescence lifetime tomography imaging of three phantoms (*Ac*, acidic; *N*, neutral; and *B*, basic) implanted into a mouse, excitation/emission: 785:830 nm. A vertical slice from the DOT reconstructed yield (*Panel A*) and lifetime (*Panel B*) is overlaid here on a white-light image of the mouse. A threshold of 50% of local maximum has been applied to isolate each tube location. Average lifetimes for the targets are 0.95 ns (*Ac*, acidified DMSO), 1.25 ns (*N*, neat DMSO), and 1.46 ns (*B*, basified DMSO).The fluorescence lifetime of the signals are shown in pseudo colors in the online version.

of three different lifetimes, suggesting three distinct environments (Fig. 5 *B*). Quantitative analysis of lifetime bands for each phantom showed good agreement with in vitro results (Table 2). The lifetime of the acidic phantom, determined tomographically, was shortest at ~0.96 ns, followed by an intermediate lifetime of ~1.25 ns in neat DMSO (pH = 5.7), and ~1.46 ns in the basic tube.

To determine the lifetimes, we modeled light propagation using the diffusion equation, explicitly taking into account the background scattering and absorption. The reconstruction process essentially assessed the amount of light (yield dominant) and phase delay (lifetime dominant) in each measurement and from a group of such measurements, determined the most likely three-dimensional map of fluorophore properties. At the regions where the tubes were placed in the mouse, we assumed homogeneous tissue optical properties (45). Although this approach produced a reasonable lifetime map, incorporation of the local map of heterogeneous tissue optical properties would more accurately delineate the in vivo lifetimes. As long as the estimates of optical properties are correct, the reconstruction method used in this study deconvolves the scattering process from the fluorophore lifetime. In a previous study, we demonstrated that in vivo lifetime measurements of NIR fluorophores were within 10% of their values in solution (26).

DISCUSSION

Mechanism of pH sensitivity

At extreme pH environments, cyanine dyes typically display pH-sensitivity through large spectral shifts but these extremes are not valuable for biological imaging. Recent studies have shown that some cyanine dyes can exhibit significant changes in fluorescence intensity as a function of pH but we are not aware of studies reporting the development and use of NIR fluorescent lifetime pH-sensitive dyes. To delineate the contribution of cyanine structural framework to the observed pH-response of both LS479 and LS482, we analyzed the pH-dependent properties of their parent dye, HITC (Fig. 1). The three dyes share the same hexamethylindotricarbocyanine skeleton responsible for their NIR fluorescence.

However, the HITC structure does not have similar acid-base sensitive functionalities or solvation centers as LS479 and LS482. Consequently, it is not expected to be pH-sensitive within a physiologically relevant range. Indeed, the pH-sensitivity of HITC was negligible in the NIR region (Fig. S2, *A* and *B*). This resulted in a marginal change in quantum yield (Table 1). Consequently, the fluorescence decays of HITC at three different media (acidic, neutral, and basic DMSO) remained primarily monoexponential (~100% of one component from a two-exponential fit) with the same lifetime 1.42–1.43 ns (Table 2). The lack of pH-sensitivity by HITC supports the hypothesis that the presence of amine functionality on LS479 and LS482 conferred steady-state fluorescence and, in the case of LS482, lifetime pH-sensitivity.

Previously, we reported that complexation of Zn^{2+} to LS479 significantly enhanced the fluorescence quantum yield of the fluorophore. We explained the enhancement through an excited-state charge transfer (ESCT) mechanism (46). According to the proposed mechanism, Zn^{2+} acts as a Lewis acid and attracts a lone pair, suppressing ESCT. Protonation of the amine group was also expected to suppress ESCT and enhance fluorescence (14,47,48). However, the opposite trend was actually observed: protonation of LS479 and LS482 caused significant reduction in quantum yields and, in the case of LS482, in the fluorescence lifetime. Similar effect was also noticed by Peng et al. (38), although it was not clear whether that was due to fluorescence quenching or change in absorbance. Preliminary computational analysis (not shown here) revealed that upon nitrogen protonation in LS479 and LS482, the negative charge on the nitrogen atom in the ground state becomes larger, suggesting that the electron pair migrates closer to nitrogen. Enlarged electron density could participate in ESCT and effectively

suppress fluorescence. The computational work is currently under way and will be reported separately.

Due to the presence of metal chelating group, the compounds LS479 and LS482 might not be suitable for in vivo imaging applications of tissues with substantial level of metals. Chelation is likely to affect the pK_a of the dyes; for example, LS479-metal complexes are insensitive to the changes in pH in physiological range (data are not shown). Hence, the design of the probes has to be further tuned to eliminate potential complexation of the dyes with metals.

Strategies for developing lifetime pH-sensitive probe

For a compound to be a lifetime pH-sensitive probe, certain criteria have to be met:

1. The fluorescence has to be pH-sensitive, requiring the formation of two emission species.
2. The fluorescence lifetime of protonated and deprotonated species have to be distinct.
3. The lifetime should not be affected by other species, like metals.
4. Both protolytic forms must emit in the same range, ideally with almost complete spectral overlap.

Although the former three requirements are obvious, the last one necessitates an additional explanation.

Consider the Henderson-Hasselbach equation (49) for a pH-sensitive fluorophore formed as a result of a protolytic reaction in the excited state,

$$AH^* \underset{+H^{\oplus}}{\overset{-H^{\oplus}}{\rightleftharpoons}} A^*,$$

$$\mathrm{pH} = \mathrm{pK_a^*} - \log\left(\frac{[AH]^*}{[A]^*}\right), \tag{1}$$

where $[AH]^*$ is the concentration of a protonated form in the excited state, $[A]^*$ is the concentration of a deprotonated form in the excited state, and pK_a^* is the acid dissociation constant in the excited state.

The fraction contribution of both forms can be expressed via their excited concentrations, molar absorptivities, and quantum yields from Eq. 2,

$$f_i = \frac{[f_i](\varepsilon_i \times \psi_i)}{\sum_i^n [f_i](\varepsilon_i \times \psi_i)}, \tag{2}$$

where $[f_i]$ values are the concentrations of each component in the excited state, f_i is the fractional component obtained from fluorescence n-exponential fit decay analysis, n is the number of fractional components, ε_i is the molar absorptivity of each component at the wavelength of excitation, and ψ_i is the fluorescence quantum yield.

Thus, for a protolytic reaction, the concentrations of the protonated and deprotonated forms in the excited state are

$$f_{AH} = \frac{[AH^*](\varepsilon_{AH} \times \psi_{AH})}{[AH^*](\varepsilon_{AH} \times \psi_{AH}) + [A^*](\varepsilon_A \times \psi_A)}, \tag{3}$$

$$f_A = \frac{[AH^*](\varepsilon_A \times \psi_A)}{[AH^*](\varepsilon_{AH} \times \psi_{AH}) + [A^*](\varepsilon_A \times \psi_A)}, \tag{4}$$

where ε_{AH} and ε_A are molar absorptivity of protonated and deprotonated forms at the wavelength of excitation, and ψ_{AH} and ψ_A are fluorescence quantum yields of protonated and deprotonated forms.

Dividing Eq. 4 by Eq. 3, we have

$$\frac{f_{AH}}{f_a} = \frac{[AH^*](\varepsilon_{AH} \times \psi_{AH})}{[A^*](\varepsilon_A \times \psi_A)}. \tag{5}$$

Rearranging of Eq. 5 gives:

$$\frac{[AH^*]}{[A^*]} = \frac{f_{AH}(\varepsilon_{AH} \times \psi_{AH})}{f_a(\varepsilon_A \times \psi_A)}. \tag{6}$$

Combining Eqs. 1 and 6:

$$\mathrm{pH} = \mathrm{pK_a^*} - \log_{10}\left(\frac{\varepsilon_A \times \psi_A}{\varepsilon_{AH} \times \psi_{AH}} \times \frac{f_{AH}}{f_A}\right). \tag{7}$$

The measured fluorescence lifetime $\tilde{\tau}$ from a two-exponential fit could be expressed by Eq. 8, as

$$\tilde{\tau} = f_A\tau_A + f_{AH}\tau_{AH},\ f_A + f_{AH} = 1, \tag{8}$$

where f_A and f_{AH} are the fractional contributions of the deprotonated and protonated forms, τ_A and τ_{AH} are the fluorescence lifetimes for each emitting state.

It can readily be shown from Eq. 8 that the ratio of the two fractional contributions can be expressed as given in Eq. 9:

$$\frac{f_{AH}}{f_A} = \frac{\tilde{\tau} - \tau_A}{\tau_{AH} - \tilde{\tau}}. \tag{9}$$

Combining Eqs. 7 and 9 gives Eq. 10 for measuring pH from steady-state parameters and fluorescence lifetimes determined for each individual protonated and deprotonated species:

$$\mathrm{pH} = \mathrm{pK_a^*} - \log_{10}\left(\frac{\varepsilon_A \times \psi_A}{\varepsilon_{AH} \times \psi_{AH}}\right) - \log_{10}\left(\frac{\tilde{\tau} - \tau_A}{\tau_{AH} - \tilde{\tau}}\right). \tag{10}$$

From here, we can postulate the expression of Henderson-Hasselbach equation for lifetime measurements given in Eq. 11. Good correlation between the predicted curve from Eq. 11 and experimental data observed (Fig. S4) support our postulate, with

$$\mathrm{pH} = \mathrm{pK_{a,\tau}^*} - \log_{10}\left(\frac{\tilde{\tau} - \tau_A}{\tau_{AH} - \tilde{\tau}}\right), \tag{11}$$

where

$$pK^*_{a,\tau} = pK^*_a - \log_{10}\left(\frac{\varepsilon_A \times \psi_A}{\varepsilon_{AH} \times \psi_{AH}}\right)$$

and where $pK^*_{a,\tau}$ is the acid dissociation constant determined from lifetime measurements.

Similar to the acid dissociation constant for the excited state pK^*_a, the $pK^*_{a,\tau}$ depends on the fluorescence brightness of the protolytic forms ($\varepsilon_i \times \psi_i$), and therefore on the wavelength of excitation. For molecules with similar brightness values, both pK_a parameters become equal ($pK^*_{a,\tau} \approx pK^*_a$) and the pH of the unknown system can be determined directly from the measured lifetimes.

Equation 11 has an important implication in predicting whether the probe is suitable as a lifetime pH-sensitive probe. If one of the protolytic forms is significantly shifted (>200 nm as with norcyanines (50,51)), then the molar absorptivity at the wavelength of excitation would be insignificant ($\varepsilon_i \rightarrow 0$), leading to a very large discrepancy between $pK^*_{a,\tau}$ and pK^*_a and loss of lifetime sensitivity. Similarly, if one of the forms is nonfluorescent (quantum yield $\psi_i \rightarrow 0$), the lifetime sensitivity is also negligible. LS482 has a relatively small bathochromic spectral shift upon protonation with both forms absorbing and emitting within narrow NIR range, and hence exhibits fluorescence lifetime sensitivity.

Molecular probes that meet the above requirements have additional advantages for in vivo molecular imaging. Because the spectral shifts are small, leading to significant fluorescence spectral overlap between protonated and nonprotonated forms, in vivo ratiometric measurements will be difficult. In this case, the unique characteristic of lifetime parameter conveniently allows the two species to be delineated with ease. Moreover, single excitation and detection wavelengths can be used for imaging the pH status of tissue. This strategy minimizes the complexity of instrumentation needed for FL-DOT studies. It must be noted that the absorption and emission properties of dye LS482 are not optimal under the in vivo experimental conditions utilized in this work. To optimize the fixed excitation wavelength of our present FL-DOT system, future studies will use pH-sensitive FLT dyes prepared for excitation at 785 nm. An alternative strategy is to use lasers with different excitation outputs, although such systems tend to be more expensive.

CONCLUSIONS

In summary, this study reports the concept of pH-sensitive fluorescence lifetime molecular probes for potential applications in vivo. Particularly, we showed that electronically coupling an amino group to the fluorophore of a pH-insensitive dye, HITC, produced pH-sensitive compounds. The pK_a of the dyes critically depends on the location of the substitution along the cyanine chromophore core. Peripheral substitution at the 5-position of the indole ring resulted in a compound (LS479) with $pK_a \sim 4.9$, which is less optimal for biological imaging studies. However, shifting the substitution to the meso-position produced a fluorophore (LS482) with a pK_a of 5.5. Additionally, LS482 demonstrated lifetime pH-sensitivity originating from distinct lifetimes for the protonated (~1.16 ns in acidic DMSO) and deprotonated (~1.40 ns in basic DMSO) components. Although the design of the probes has to be further tuned to eliminate potential complexation of the dyes with endogenous metals, the feasibility of the lifetime sensitivity in vivo imaging was demonstrated. The simulated mouse model was developed and the lifetime values measured with FL-DOT system were in a good agreement with the values obtained in cuvettes. Such agreement provides a unique opportunity to develop optimal NIR molecular probes and FL-DOT system for detecting and diagnosing acidosis-related diseases.

SUPPORTING MATERIAL

One diagram and four figures are available at http://www.biophysj.org/biophysj/supplemental/S0006-3495(11)00302-X.

This work was supported primarily by the National Institute of Biomedical Imaging and Bioengineering under grant No. RO1EB007276, and in part by other funds by the National Institutes of Health under grants No. R01 EB008111, No. R01 EB001430, No. R01 EB008458, No. R01 CA109754, No. R33 CA123537, and No. R21 CA149814 as well as the the NIH Roadmap for Medical Research as funding source for the IPDC, and the Intramural Research Program of Eunice Shriver NICHD.

REFERENCES

1. Glaasker, E., W. N. Konings, and B. Poolman. 1996. The application of pH-sensitive fluorescent dyes in lactic acid bacteria reveals distinct extrusion systems for unmodified and conjugated dyes. *Mol. Membr. Biol.* 13:173–181.
2. Dellian, M., G. Helmlinger, …, R. K. Jain. 1996. Fluorescence ratio imaging of interstitial pH in solid tumors: effect of glucose on spatial and temporal gradients. *Br. J. Cancer.* 74:1206–1215.
3. Kondo, T., and S. Hirohashi. 2006. Application of highly sensitive fluorescent dyes (CyDye DIGE Fluor saturation dyes) to laser microdissection and two-dimensional difference gel electrophoresis (2D-DIGE) for cancer proteomics. *Nat. Protoc.* 1:2940–2956.
4. Gennari, F. J. e. 2005. Acid-Base Disorders and their Treatment. Taylor & Francis, Boca Raton, FL.
5. Tannock, I. F., and D. Rotin. 1989. Acid pH in tumors and its potential for therapeutic exploitation. *Cancer Res.* 49:4373–4384.
6. Wike-Hooley, J. L., A. P. van den Berg, …, H. S. Reinhold. 1985. Human tumor pH and its variation. *Eur. J. Cancer Clin. Oncol.* 21:785–791.
7. Fukumura, D., and R. K. Jain. 2008. Imaging angiogenesis and the microenvironment. *APMIS.* 116:695–715.
8. Boron, W. F., and E. L. Boulpaep. 2009. Medical Physiology: A Cellular and Molecular Approach. Saunders/Elsevier, Philadelphia, PA.
9. Zhang, W., B. Tang, …, G. Yang. 2009. A highly sensitive acidic pH fluorescent probe and its application to HepG2 cells. *Analyst (Lond.).* 134:367–371.
10. Almutairi, A., S. J. Guillaudeu, …, J. M. Fréchet. 2008. Biodegradable pH-sensing dendritic nanoprobes for near-infrared fluorescence lifetime and intensity imaging. *J. Am. Chem. Soc.* 130:444–445.

11. Lee, H., M. Y. Berezin, …, S. Achilefu. 2009. Near-infrared fluorescent pH-sensitive probes via unexpected barbituric acid mediated synthesis. *Org. Lett.* 11:29–32.
12. Zhang, Z., and S. Achilefu. 2005. Design, synthesis and evaluation of near-infrared fluorescent pH indicators in a physiologically relevant range. *Chem. Commun. (Camb.).* 47:5887–5889.
13. Deniz, E., G. C. Isbasar, …, E. U. Akkaya. 2008. Bidirectional switching of near IR emitting boradiazaindacene fluorophores. *Org. Lett.* 10:3401–3403.
14. Hilderbrand, S. A., K. A. Kelly, …, R. Weissleder. 2008. Near infrared fluorescence-based bacteriophage particles for ratiometric pH imaging. *Bioconjug. Chem.* 19:1635–1639.
15. Tang, B., F. Yu, …, X. Wang. 2009. A near-infrared neutral pH fluorescent probe for monitoring minor pH changes: imaging in living HepG2 and HL-7702 cells. *J. Am. Chem. Soc.* 131:3016–3023.
16. Han, J., and K. Burgess. 2010. Fluorescent indicators for intracellular pH. *Chem. Rev.* 110:2709–2728.
17. Kuwana, E., F. Liang, and E. M. Sevick-Muraca. 2004. Fluorescence lifetime spectroscopy of a pH-sensitive dye encapsulated in hydrogel beads. *Biotechnol. Prog.* 20:1561–1566.
18. Sevick-Muraca, E. M., J. P. Houston, and M. Gurfinkel. 2002. Fluorescence-enhanced, near infrared diagnostic imaging with contrast agents. *Curr. Opin. Chem. Biol.* 6:642–650.
19. Hassan, M., J. Riley, …, A. H. Gandjbakhche. 2007. Fluorescence lifetime imaging system for in vivo studies. *Mol. Imaging.* 6:229–236.
20. Kumar, A. T., J. Skoch, …, A. K. Dunn. 2005. Fluorescence-lifetime-based tomography for turbid media. *Opt. Lett.* 30:3347–3349.
21. Maule, C., H. Gonçalves, …, P. Jorge. 2010. Wavelength encoded analytical imaging and fiber optic sensing with pH sensitive CdTe quantum dots. *Talanta.* 80:1932–1938.
22. Liu, Y., H. R. Kim, and A. A. Heikal. 2006. Structural basis of fluorescence fluctuation dynamics of green fluorescent proteins in acidic environments. *J. Phys. Chem. B.* 110:24138–24146.
23. Berezin, M. Y., H. Lee, …, S. Achilefu. 2007. Near infrared dyes as lifetime solvatochromic probes for micropolarity measurements of biological systems. *Biophys. J.* 93:2892–2899.
24. Lee, H., M. Y. Berezin, …, S. Achilefu. 2008. Fluorescence lifetime properties of near-infrared cyanine dyes in relation to their structures. *J. Photochem. Photobiol. Chem.* 200:438–444.
25. Gota, C., S. Uchiyama, …, T. Ohwada. 2008. Temperature-dependent fluorescence lifetime of a fluorescent polymeric thermometer, poly (N-isopropylacrylamide), labeled by polarity and hydrogen bonding sensitive 4-sulfamoyl-7-aminobenzofurazan. *J. Phys. Chem. B.* 112:2829–2836.
26. Nothdurft, R. E., S. V. Patwardhan, …, J. P. Culver. 2009. In vivo fluorescence lifetime tomography. *J. Biomed. Opt.* 14:024004.
27. Patwardhan, S. V., S. R. Bloch, …, J. Culver. 2005. Time-dependent whole-body fluorescence tomography of probe bio-distributions in mice. *Opt. Express.* 13:2564–2577.
28. Berezin, M. Y., K. Guo, …, S. Achilefu. 2009. Radioactivity-synchronized fluorescence enhancement using a radionuclide fluorescence-quenched dye. *J. Am. Chem. Soc.* 131:9198–9200.
29. Benson, R. C., and H. A. Kues. 1978. Fluorescence properties of indocyanine green as related to angiography. *Phys. Med. Biol.* 23:159–163.
30. Kiyose, K., H. Kojima, …, T. Nagano. 2006. Development of a ratiometric fluorescent zinc ion probe in near-infrared region, based on tricarbocyanine chromophore. *J. Am. Chem. Soc.* 128:6548–6549.
31. Ntziachristos, V., and R. Weissleder. 2001. Experimental three-dimensional fluorescence reconstruction of diffuse media by use of a normalized Born approximation. *Opt. Lett.* 26:893–895.
32. O'Leary, M. A., D. A. Boas, …, A. G. Yodh. 1996. Fluorescence lifetime imaging in turbid media. *Opt. Lett.* 21:158–160.
33. Haskell, R. C., L. O. Svaasand, …, B. J. Tromberg. 1994. Boundary conditions for the diffusion equation in radiative transfer. *J. Opt. Soc. Am. A Opt. Image Sci. Vis.* 11:2727–2741.
34. Guo, K., M. Y. Berezin, …, S. Achilefu. 2010. Near infrared-fluorescent and magnetic resonance imaging molecular probe with high T1 relaxivity for in vivo multimodal imaging. *Chem. Commun. (Camb.).* 46:3705–3707.
35. Kanofsky, J. R., and P. D. Sima. 2000. Structural and environmental requirements for quenching of singlet oxygen by cyanine dyes. *Photochem. Photobiol.* 71:361–368.
36. Loura, L. M., A. Fedorov, and M. Prieto. 1996. Resonance energy transfer in a model system of membranes: application to gel and liquid crystalline phases. *Biophys. J.* 71:1823–1836.
37. Goiffon, R. J., W. J. Akers, …, S. Achilefu. 2009. Dynamic noninvasive monitoring of renal function in vivo by fluorescence lifetime imaging. *J. Biomed. Opt.* 14:020501.
38. Peng, X., F. Song, …, Y. Gao. 2005. Heptamethine cyanine dyes with a large Stokes shift and strong fluorescence: a paradigm for excited-state intramolecular charge transfer. *J. Am. Chem. Soc.* 127:4170–4171.
39. Allen, M. W., J. R. Unruh, …, C. K. Johnson. 2003. Spectroscopy and photophysics of indoline and indoline-2-carboxylic acid. *J. Phys. Chem. A.* 107:5660–5669.
40. Polster, J., and H. Lachmann. 1989. Spectrometric Titrations: Analysis of Chemical Equilibria. VCH Verlagsgesellschaft, Weinheim, Germany.
41. Agmon, N. 2005. Elementary steps in excited-state proton transfer. *J. Phys. Chem. A.* 109:13–35.
42. Tolbert, L. M., and K. M. Solntsev. 2002. Excited-state proton transfer: from constrained systems to "super" photoacids to superfast proton transfer. *Acc. Chem. Res.* 35:19–27.
43. Berezin, M. Y., and S. Achilefu. 2010. Fluorescence lifetime measurements and biological imaging. *Chem. Rev.* 110:2641–2684.
44. Akers, W. J., M. Y. Berezin, …, S. Achilefu. 2008. Predicting in vivo fluorescence lifetime behavior of near-infrared fluorescent contrast agents using in vitro measurements. *J. Biomed. Opt.* 13:054042.
45. Patwardhan, S. V., and J. P. Culver. 2008. Quantitative diffuse optical tomography for small animals using an ultrafast gated image intensifier. *J. Biomed. Opt.* 13:011009.
46. Berezin, M. Y., W. J. Akers, …, S. Achilefu. 2009. Long fluorescence lifetime molecular probes based on near infrared pyrrolopyrrole cyanine fluorophores for in vivo imaging. *Biophys. J.* 97:L22–L24.
47. Lakowicz, J. R. 2006. Principles of Fluorescence Spectroscopy. Springer, New York.
48. Hilderbrand, S. A., and R. Weissleder. 2007. Optimized pH-responsive cyanine fluorochromes for detection of acidic environments. *Chem. Commun. (Camb.).* 26:2747–2749.
49. Seibert, E., A. S. Chin, …, J. B. A. Ross. 2003. pH-Dependent spectroscopy and electronic structure of the guanine analog 6,8-dimethylisoxanthopterin. *J. Phys. Chem. A.* 107:178–185.
50. Encinas, C., E. Otazo, …, J. Alonso. 2002. Croconines: new acidochromic dyes for the near infrared region. *Tetrahedron Lett.* 43:8391–8393.
51. Miltsov, S., C. Encinas, and J. N. Alonso. 1998. Nortricarbocyanines: new near-infrared pH-indicators. *Tetrahedron Lett.* 39:9253–9254.